Latin American Journal of Solids and Structures
www.lajss.org

Buckling of Slender Concrete-Filled Steel Tubes with Compliant Interfaces

Abstract

This paper presents an exact model for studying the global buckling of concrete-filled steel tubular (CFST) columns with compliant interfaces between the concrete core and steel tube. This model is then used to evaluate exact critical buckling loads and modes of CFST columns. The results prove that interface compliance can considerably reduce the critical buckling loads of CFST columns. A good agreement between analytical and experimental buckling loads is obtained if at least one among longitudinal and radial interfacial stiffnesses is high. The parametric study reveals that buckling loads of CFST columns are very much affected by the interfacial stiffness and boundary conditions.

Keywords

Buckling, composite column, steel tubes, concrete-filled

Simon Schnabl [a, *]
Igor Planinc [b]

[a] University of Ljubljana, Faculty of Chemistry and Chemical Technology, Večna pot 113, 1001 Ljubljana, Slovenia
E-mail address: simon.schnabl@fkkt.uni-lj.si
[b] University of Ljubljana, Faculty of Civil and Geodetic Engineering, Jamova 2, 1000 Ljubljana, Slovenia
E-mail address: igor.planinc@fgg.uni-lj.si

* Corresponding author

http://dx.doi.org/10.1590/1679-78253479

Received 01.11.2016
In revised form 13.02.2017
Accepted 23.03.2017
Available online 27.03.2017

NOMENCLATURE

A cross-sectional area (cm^2)
C radial contact stiffness (kN/cm^2)
D outer diameter of the steel tube (mm)
E elastic modulus (kN/cm^2)
I moment of inertia (cm^4)
K longitudinal contact stiffness (kN/cm^2)
L column length (cm)

NOMENCLATURE (continuation)

M_Y cross-sectional bending moment (kNcm)
P centrally applied point force (kN)
P_{cr} critical buckling load (kN)
p_X contact traction in X direction (kN/cm^2)
p_Z contact traction in Z direction (kN/cm^2)
m_Y contact traction in Y direction (kNcm/cm^2)
R_X X component of the cross-sectional equilibrium force (kN)
R_Z Z component of the cross-sectional equilibrium force (kN)
t wall thickness of the steel tube (mm)
u axial displacement (cm)
w deflection (cm)

Greek letters

δ variation operator
Δ_U interlayer slip (cm)
Δ_W interlayer uplift (cm)
ε axial strain
$\varepsilon_{\mathrm{cr}}$ critical axial strain
κ pseudocurvature (rad/m)
λ column slenderness ratio
φ rotation (rad)

Superscripts

i layer or material
c concrete core
s steel tube

1 INTRODUCTION

Concrete-filled steel tubular (CFST) columns are becoming popular in today's construction practice. They are used in many structural applications including columns supporting platforms of offshore structures and wind turbines, roofs of storage tanks, bridge piers, piles, and columns in seismic zones and high-rise buildings. CFST columns offer major advantages over either pure steel tubes or concrete members. Stiffness, strength, ductility, seismic and fire resistance, deformation characteristics, elimination of formwork costs, installation, economy, and good performance are among the advantages achieved in using such a structural system.

Accordingly, a great deal of experimental research works has been done by Zeghiche and Chaoui (2005), Ellobody et al. (2006), Yang and Han (2006), Guo et al. (2007), Lai and Ho (2014), Feng et al. (2015), and Wang et al. (2015) among many others, to investigate the behaviour of CFST columns. Alternatively, much numerical research work has been reported by Shams and Saadeghvaziri (1999), Hu et al. (2003), Valipour and Foster (2010), Liang (2011), Tao et al. (2013), Wang and

Young (2013), Patel et al. (2014), Zhang et al. (2015), Aslani et al. (2015), and analytical studies by Choi and Xiao (2010), Schneider (1998), Brauns (1999), Susantha et al. (2001), Fam et al. (2004), Kuranovas et al. (2009). An up to date review on steel-concrete composite columns including experimental and analytical studies has been reported by Shanmugam and Lakshimi (2001). Likewise, Han et al. (2014) have reviewed the development and advanced applications of the family of CFST structures till today.

CFST columns can sustain large axial loads especially when used in high-rise buildings. Shorter CFST columns may fail by crushing of the concrete core or by local buckling and yielding of the steel tube, while on the other hand, slender CFST columns usually fail by overall buckling. Most of the research on CFST columns covered in the literature is focused on short CFST columns. However, much less literature is available on global buckling behaviour of slender CFST columns. Thus, only a few papers have dealt with this subject, see e.g. Goode et al. (2010), Romero et al. (2011), Portoles et al. (2011), Dai et al. (2014), and Hassanein and Kharoob (2014). Note, that to date, only Han (2000) has experimentally investigated the buckling behavior of circular CFST columns with very high slenderness ratios.

The above-mentioned research work done on CFST columns is based on a simple prediction of fully bonded connection between the concrete core and the steel tube. Nevertheless, in real situations, imperfect interface compliance between the concrete core and the steel tube is observed especially when high axial loads are considered. Unfortunately, this imperfect bonding can reduce the initial stiffness and elastic strength of CFST columns considerably. The situation can be even worse in case of high-strength CFST columns, see Liao et al. (2011). Despite that, research works on composite action in CFST columns are still very limited in literature. To date, only a few researchers have studied composite action in CFST columns; see e.g. Liao et al. (2011), Hajjar et al. (1998), Fam et al. (2004), Roeder et al. (2010). In all of these studies, it has been shown that composite action in CFST columns is not well understood and thus remains as an interesting topic for future research.

The main purpose of this paper is the continuation work (Schnabl and Planinc, 2015) done on the formulation of analytical model for studying the buckling behaviour of CFST composite columns with compliant interface between the concrete core and steel tube. Thus, the derived mathematical model is based on the mechanics of layered column theories recently developed by Schnabl et al. (2007), Schnabl and Planinc (2010, 2011a, 2011b, 2013), and Kryžanowski et al. (2008, 2014). The analytical model is then used in the numerical examples to show its applicability for the analysis of buckling behavior of CFST columns with compliant interface and different boundary conditions.

2 PROBLEM FORMULATION

2.1 CFST Column under Consideration

An initially straight, planar, geometrically perfect CFST circular column as shown in Figure 1 is considered. The CFST column has an undeformed length L and is made from a concrete core, c, and a steel tube, s, joined by an interface of negligible thickness and finite stiffness in normal and tangential directions. The CFST circular column is placed in the (X,Z) plane of a spatial Cartesian coordinate system with coordinates (X,Y,Z) and unit base vectors $\boldsymbol{E}_X$, $\boldsymbol{E}_Y$ and $\boldsymbol{E}_Z = \boldsymbol{E}_X \times \boldsymbol{E}_Y$. The

undeformed reference axis of the CFST circular column is common to both layers. It is parameterized by the undeformed arc-length x. Material particles of the concrete core and the steel tube are identified by material coordinates (x^i, y^i, z^i), $(i = c, s)$ in local coordinate system which is assumed to coincide initially with spatial coordinates, and then follows the deformation of the column. Thus, $(x^i = x = X)$, $(y^i = y = Y)$, and $(z^i = z = Z)$ in the undeformed configuration. Further, each material is modelled by Reissner's large-displacement finite-strain shear-undeformable beam theory (Reissner, 1972). The CFST circular column is subjected to a conservative compressive load, P, which acts along the neutral axis of the CFST circular column in such a way that homogeneous stress-strain state of the CFST column in its primary configuration is achieved. For more details on buckling behavior of composite columns an interested reader is referred to the work of Kryžanowski et al. (2009, 2014), Schnabl and Planinc (2010, 2011a, 2011b, 2013}.

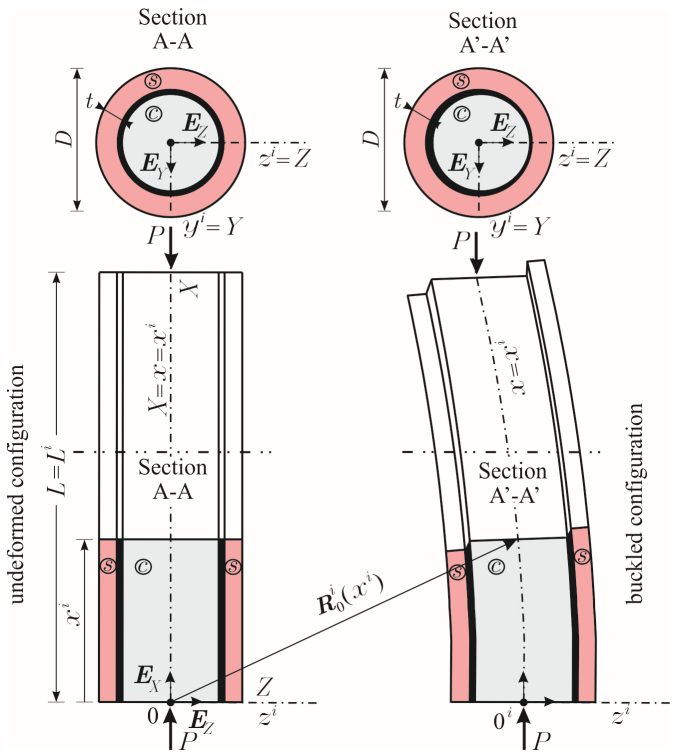

Figure 1: Initial and buckled configuration of circular CFST column.

2.2 Assumptions

In addition to the abovementioned assumptions, a mathematical formulation of governing equations of a circular CFST column is based on the following assumptions:

1. The material is linear elastic.
2. The planar Reissner beam theory (Reissner, 1972) is used for each material.
3. The shear deformations are not taken into account.
4. No local type of instability can occur

5. The materials can slip over each other and separate in radial direction.
6. The materials are continuously connected and slip and uplift moduli of the connection are constant.
7. The shapes of the materials' cross-sections are symmetrical with respect to the plane of deformation and remain unchanged in the form and size during deformation.
8. The interlayer slip and uplift are small.
9. The CFST column is slender.

2.3 Nonlinear Governing Equations

Nonlinear governing equations of a CFST circular column is composed of kinematic, equilibrium, and constitutive equations along with natural and essential boundary conditions for each of the material. Furthermore, there are also constraining equations which assemble each individual material into a composite structure. A compact notation $(\bullet)^i$ will be used in further expressions, where $i = (c,s)$ indicates to which layer the quantity $(\bullet)$ belongs to. The governing nonlinear equations of a CFST circular column constitute a system of 12 first order differential equations with constant coefficients for 12 unknown functions $u^i, w^i, \varphi^i\, w^i,\ R_X^i,\ R_Z^i,\ M_Y^i$:

Kinematic equations

$$1 + \frac{du^i}{dx} - (1+\varepsilon^i)\cos\varphi^i = 0, \tag{1}$$

$$\frac{dw^i}{dx} + (1+\varepsilon^i)\sin\varphi^i = 0, \tag{2}$$

$$\frac{d\varphi^i}{dx} - \kappa^i = 0, \tag{3}$$

Equilibrium equations

$$\frac{dR_X^i}{dx} + p_X = 0, \tag{4}$$

$$\frac{dR_Z^i}{dx} + p_Z = 0, \tag{5}$$

$$\frac{dM_Y^i}{dx} - (1+\varepsilon^i)(R_X^i \sin\varphi^i + R_Z^i \cos\varphi^i) + m_Y = 0, \tag{6}$$

Constitutive equations

$$R_X^i \cos\varphi^i - R_Z^i \sin\varphi^i - E^i A^i \varepsilon^i = 0, \tag{7}$$

$$M_Y^i - E^i I^i \kappa^i = 0. \tag{8}$$

Natural and essential boundary conditions

$x^i = 0$

$$\begin{aligned} S_1^i + R_X^i(0) &= 0 \qquad \text{or} \qquad u^i(0) = u_1^i, \\ S_2^i + R_Z^i(0) &= 0 \qquad \text{or} \qquad w^i(0) = u_2^i, \\ S_3^i + M_Y^i(0) &= 0 \qquad \text{or} \qquad \varphi^i(0) = u_3^i. \end{aligned} \tag{9}$$

$x^i = L$

$$\begin{aligned} S_4^i + R_X^i(L) &= 0 \qquad \text{or} \qquad u^i(L) = u_4^i, \\ S_5^i + R_Z^i(L) &= 0 \qquad \text{or} \qquad w^i(L) = u_5^i, \\ S_6^i + M_Y^i(L) &= 0 \qquad \text{or} \qquad \varphi^i(L) = u_6^i. \end{aligned} \tag{10}$$

u_k^i and S_k^i (k=1,2,...,6) mark given values of generalized boundary displacements and their complementary generalized forces at the edges of materials, i.e. $x^i = 0$ and $x^i = L$, respectively.

Constraining equations and contact model

In case of a CFST column a material s is constrained to follow the deformation of the material c, and vice versa, which means that displacements of initially coincident material particles in the contact are constrained to each other. This kinematic-constraint relation can be expressed with the positions of the observed material particles in the deformed configuration

$$\boldsymbol{R}^i = X^i \boldsymbol{E}_X + Y^i \boldsymbol{E}_Y + Z^i \boldsymbol{E}_Z, \tag{11}$$

where the spatial Cartesian coordinates $X^i, Y^i,$ and Z^i are dependent on the generalized displacements $u^i, w^i,$ and φ^i as

$$X^i = x + u^i - r\sin\alpha\sin\varphi^i, \tag{12}$$

$$Y^i = r\cos\alpha, \tag{13}$$

$$Z^i = w^i - r\sin\alpha\cos\varphi^i. \tag{14}$$

A displacement vector $[[\boldsymbol{R}]]$ between the two initially coincident material particles that belong to material c and s, respectively, is given as a vector-valued function by

$$\left[\left[\boldsymbol{R}\right]\right] = \boldsymbol{R}^c - \boldsymbol{R}^s = \Delta_U \boldsymbol{E}_X + \Delta_W \boldsymbol{E}_Z, \tag{15}$$

or in component form as

$$\Delta_U(x,\alpha) = u^c - u^s - r\sin\alpha(\sin\varphi^c - \sin\varphi^s), \tag{16}$$

$$\Delta_W(x,\alpha) = w^c - w^s - r\sin\alpha(\cos\varphi^c - \cos\varphi^s), \tag{17}$$

where Δ_U and Δ_W are the interlayer slip and uplift between the observed material particles with respect to $\boldsymbol{E}_X$ and $\boldsymbol{E}_Z$, and r and α are the polar coordinates of the observed material particle in the contact, see Figure 2.

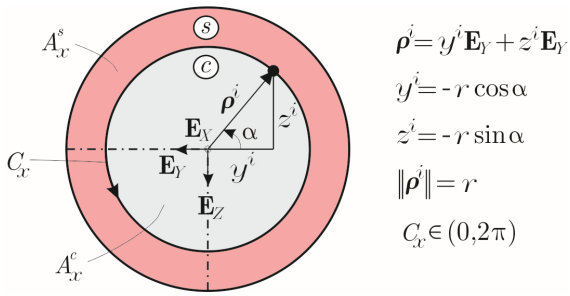

Figure 2: Cross-section of a circular CFST column.

As a consequence of (15) or (16)-(17), interlayer contact tractions emerge whose magnitudes depend on the type of the connection. Hence, the contact tractions per unit of the undeformed reference axis of a CFST circular column are expressed as

$$p_X = \int_{C_x} F(\Delta_U)\mathrm{d}C_x = \int_0^{2\pi} F(\Delta_U) r \mathrm{d}\alpha, \tag{18}$$

$$p_Z = \int_{C_x} G(\Delta_W)\mathrm{d}C_x = \int_0^{2\pi} G(\Delta_W) r \mathrm{d}\alpha, \tag{19}$$

$$m_Y = \int_{C_x} \boldsymbol{\rho}^i \times \big(F(\Delta_U), 0, G(\Delta_W)\big)\mathrm{d}C_x = \int_0^{2\pi} (0, -r\cos\alpha, -r\sin\alpha) \times \big(F(\Delta_U), 0, G(\Delta_W)\big) r \mathrm{d}\alpha, \tag{20}$$

where $\boldsymbol{\rho}^i$ is the cross-sectional vector-valued position function of the observed material particle of the material i in the contact, C_x and $\mathrm{d}C_x$ are the contour and its differential of the cross-section of layer i, see Figure 2, F and G are experimentally determined (usually by push-out test) non-linear functions that describe constitutive contact laws.

2.4 Linearized Governing Equations

A linearized system of governing equations for a determination of critical buckling loads and modes of CFST columns is based on the first variation of the nonlinear system (2)-(20) defined here as

$$\delta\boldsymbol{\Psi}(\boldsymbol{x}, \delta\boldsymbol{x}) = \frac{\mathrm{d}}{\mathrm{d}\beta}\boldsymbol{\Psi}(\boldsymbol{x} + \beta\delta\boldsymbol{x})\Big|_{\beta=0}, \tag{21}$$

where $\boldsymbol{\Psi}$ is the functional, $\boldsymbol{x}$ and $\delta\boldsymbol{x}$ are the generalized displacement field and its increment, respectively, and β is a small scalar parameter. Therefore, to derive the linearized system of governing

equations for buckling problem of a CFST column, linearized equations have to be evaluated at the primary configuration in which the CFST column is straight, namely

$$\begin{aligned} &\varepsilon^i = -\frac{1}{\sum_i E^i A^i} P,\ \ \kappa^i = 0,\ \ u^i = u^i(0) - \frac{x}{\sum_i E^i A^i},\ \ w^i = 0,\ \ \varphi^i = 0,\ \ \Delta_U = 0, \\ &\Delta_W = 0,\ \ R_X^i = -\frac{E^i A^i}{\sum_i E^i A^i} P,\ \ R_Z^i = 0,\ \ M_Y^i = 0,\ p_X = 0,\ p_Z = 0,\ m_Y = 0. \end{aligned} \tag{22}$$

The linearized buckling equations are then:

$$\delta \frac{du^i}{dx} - \delta\varepsilon^i = 0, \tag{23}$$

$$\delta \frac{dw^i}{dx} + \left(1 - \frac{1}{\sum_i E^i A^i} P\right) \delta\varphi^i = 0, \tag{24}$$

$$\delta \frac{d\varphi^i}{dx} - \delta\kappa^i = 0, \tag{25}$$

$$\delta \frac{dR_X^c}{dx} - 2\pi r K(\delta u^c - \delta u^s) = 0, \tag{26}$$

$$\delta \frac{dR_X^s}{dx} + 2\pi r K(\delta u^c - \delta u^s) = 0, \tag{27}$$

$$\delta \frac{dR_Z^c}{dx} - 2\pi r C(\delta w^c - \delta w^s) = 0, \tag{28}$$

$$\delta \frac{dR_Z^s}{dx} + 2\pi r C(\delta w^c - \delta w^s) = 0, \tag{29}$$

$$\delta \frac{dM_Y^c}{dx} - \left(\frac{E^c A^c}{\sum_i E^i A^i} P\right) \delta \frac{dw^c}{dx} - \left(1 - \frac{1}{\sum_i E^i A^i} P\right) \delta R_Z^c - \pi r^3 K(\delta\varphi^c - \delta\varphi^s) = 0, \tag{30}$$

$$\delta \frac{dM_Y^s}{dx} - \left(\frac{E^s A^s}{\sum_i E^i A^i} P\right) \delta \frac{dw^s}{dx} - \left(1 - \frac{1}{\sum_i E^i A^i} P\right) \delta R_Z^s + \pi r^3 K(\delta\varphi^c - \delta\varphi^s) = 0, \tag{31}$$

$$\delta R_X^i - E^i A^i \delta\varepsilon^i = 0, \tag{32}$$

$$\delta M_Y^i - E^i I^i \delta\kappa^i = 0, \tag{33}$$

$$\delta\Delta_U = \delta u^c - \delta u^s - r\sin\alpha(\delta\varphi^c - \delta\varphi^s), \tag{34}$$

$$\delta\Delta_W = \delta w^c - \delta w^s, \tag{35}$$

where K and C are the longitudinal and radial contact stiffness, respectively. The system (23)-(35) is a system of 18 linear algebraic-differential equations of first order with constants coefficients for 18 unknown functions $\delta\varepsilon^i$, $\delta\kappa^i$, δu^i, δw^i, $\delta\varphi^i$, δR_X^i, δR_Z^i, $\delta\Delta_U$, and $\delta\Delta_W$ along with the corresponding boundary conditions

$x^i = 0$

$$\begin{aligned} S_1^i + \delta R_X^i(0) = 0 \qquad &\text{or} \qquad \delta u^i(0) = u_1^i, \\ S_2^i + \delta R_Z^i(0) = 0 \qquad &\text{or} \qquad \delta w^i(0) = u_2^i, \\ S_3^i + \delta M_Y^i(0) = 0 \qquad &\text{or} \qquad \delta\varphi^i(0) = u_3^i. \end{aligned} \tag{36}$$

$x^i = L$

$$\begin{aligned} S_4^i + \delta R_X^i(L) = 0 \qquad &\text{or} \qquad \delta u^i(L) = u_4^i, \\ S_5^i + \delta R_Z^i(L) = 0 \qquad &\text{or} \qquad \delta w^i(L) = u_5^i, \\ S_6^i + \delta M_Y^i(L) = 0 \qquad &\text{or} \qquad \delta\varphi^i(L) = u_6^i. \end{aligned} \tag{37}$$

u_k^i and S_k^i (k=1,2,...,6) mark given values of generalized boundary displacements and their complementary generalized forces at the edges of materials, i.e. $x^i = 0$ and $x^i = L$, respectively.

2.5 Exact Buckling Solution

The system (23)-(35) along with (36)-(37) can be written in compact form as a homogeneous system of 12 first order linear differential equations

$$\frac{d\boldsymbol{Y}}{dx}(x) = \boldsymbol{A}\,\boldsymbol{Y}(x) \qquad \text{and} \qquad \boldsymbol{Y}(0) = \boldsymbol{Y}_0, \tag{38}$$

where $\boldsymbol{Y}(x)$ is the eigenvector, $\boldsymbol{Y}(0)$ is the vector of unknown integration constants, and $\boldsymbol{A}$ is the constant real 12×12 matrix. The exact solution of (38) is given by; see (Perko, 2001):

$$\boldsymbol{Y}(x) = e^{\boldsymbol{A}x}\boldsymbol{Y}_0. \tag{39}$$

The unknown integration constants $\boldsymbol{Y}_0$ in (39) are obtained from (36)-(37). Hence, a system of 12 homogeneous linear algebraic equations for 12 unknown integration constants is obtained as

$$\boldsymbol{K}\,\boldsymbol{Y}_0 = \boldsymbol{0}, \tag{40}$$

where $\boldsymbol{K}$ is the tangent stiffness matrix. A non-trivial solution of (40) is obtained from the condition of singular stiffness matrix, e.i.

$$\det \boldsymbol{K} = 0, \tag{41}$$

which forms a linear eigenvalue problem for the critical buckling load P_{cr} and corresponding buckling modes of the CFST column.

3 NUMERICAL RESULTS AND DISCUSSION

3.1 Comparison with Experimental Results

The exact buckling loads of slender CFST P-P circular column calculated by the proposed model are compared with the experimental results obtained by Han (2000). The geometric and material data for six CFST columns are listed in Table 1 and shown in Figure 3.

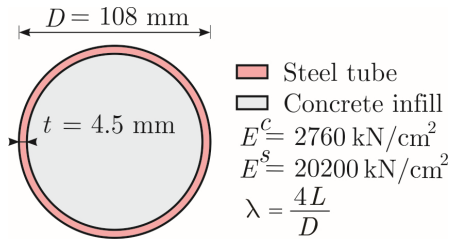

Figure 3: Geometric and material properties of CFST columns.

Exact and experimental critical buckling loads for six CFST columns are summarized in Table 1 for different K and C, and λ.

Specimen	L	λ	$N^*_{cr,e}$	C	P_{cr}					
					K=10^{-10}	K=10^{-2}	K=10^{-1}	K=1	K=10	K=10^{10}
SC154-1	415.8	154	342	10^{-10}	177.649	186.475	240.841	293.583	299.955	300.651
				10^{-5}	190.091	198.085	246.015	293.684	299.957	300.651
SC154-2	415.8	154	292	10^{-3}	295.729	295.764	296.055	297.769	300.043	300.651
SC141-1	380.7	141	350	10^{-10}	211.918	220.790	279.200	348.563	357.656	358.646
				10^{-5}	222.495	230.785	284.381	348.685	357.659	358.646
SC141-2	380.7	141	370	10^{-3}	350.255	350.326	350.909	354.103	357.762	358.646
SC130-1	351.0	130	400	10^{-10}	249.298	258.206	319.942	407.924	420.537	421.908
				10^{-5}	258.371	266.861	324.981	408.067	420.538	421.908
SC130-2	351.0	130	390	10^{-3}	408.187	408.322	409.429	415.044	420.664	421.908

* critical load obtained experimentally by Han (2000)

Table 1: Comparison of exact and experimental critical buckling loads of CFST P-P columns for various K, C, and λ, where $\varepsilon_{\mathrm{cr}} = 0$, and K and C are in kN/cm^2.

From Table 1 it can be seen that a good agreement of the results is obtained if at least one of interface stiffness (K or C) is high. Otherwise, the exact buckling loads are significantly reduced by the interface compliance. For example, the exact buckling loads are for almost fully debonded layers up to 60 % of those with completely connected to each other, and in the range of 57-64 % of exper-

imental results. Furthermore, the exact results for a relatively stiff connection ($C \geq 10^{-3}\,\mathrm{kN/cm^2}$ and $K \geq 1\mathrm{kN/cm^2}$) are within ± 10 % range measured from the mean experimental results.

3.2 Effect of Interface Compliance on Buckling Loads and Modes

A parametric study is undertaken to investigate the effect of interface compliance on critical buckling loads and modes of P-P CFST column. For this purpose, a CFST column with the same geometric and material properties as specimens SC154-1 and SC154-2 but $E^c = 2840\ \mathrm{kN/cm^2}$ is used in the parametric analysis, see Figure 3 and Table 1. The critical buckling loads are computed by the proposed exact model for various interlayer stiffnesses K and C. The results are presented in Table 2 and Figure 4.

	P_{cr}						
	C						
K	10^{-10}	10^{-7}	10^{-5}	10^{-4}	10^{-3}	10^{-2}	10^{5}
10^{-10}	179.865835$^{\bullet}$	179.993792	192.105027	255.862874	297.890147	302.479500	302.983390*
10^{-5}	179.874803	180.002752	192.113187	255.865453	297.890183	302.479501	302.983390*
10^{-3}	180.759877	180.887039	192.918146	256.119575	297.893746	302.479536	302.983390*
10^{-2}	188.553682	188.673596	199.977918	258.328044	297.925910	302.479853	302.983390*
10^{-1}	242.274702	242.329750	247.428743	273.212174	298.226557	302.483009	302.983390*
1	295.681485	295.682538	295.785453	296.603501	300.001028	302.512517	302.983390*
10	302.263327	302.263337	302.264356	302.273485	302.353467	302.687190	302.983390*
10^{2}	302.911513	302.911513	302.911524	302.911616	302.912526	302.920497	302.983390*
10^{3}	302.976203	302.976203	302.976204	302.976205	302.976214	302.976305	302.983390*
10^{5}	302.983318	302.983318	302.983318	302.983318	302.983318	302.983318	302.983390*
10^{10}	302.983390*	302.983390*	302.983390*	302.983390*	302.983390*	302.983390*	302.983390*

$^{*}P_{cr} = P_{cr}^{*}$, $^{\bullet}P_{cr} = P_{cr}^{\bullet}$

Table 2: Critical buckling loads of circular CFST P-P columns for various K, C, where $\lambda = 154$, $\varepsilon_{cr} \neq 0$, $E^c = 2840\ \mathrm{kN/cm^2}$, and C and K are in $\mathrm{kN/cm^2}$.

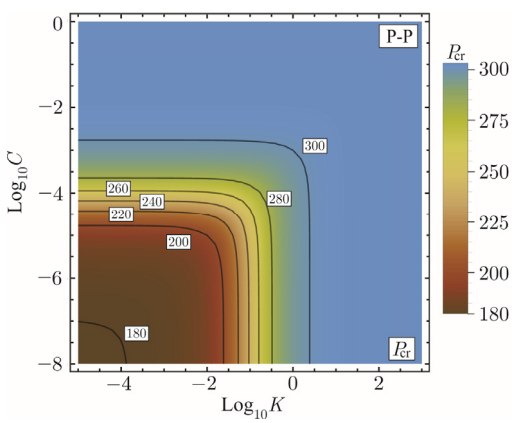

Figure 4: Density plot and contours of critical buckling load of CFST columns.

Evidently, the effect of the interface compliance on critical buckling loads of P-P CFST columns is significant. It is seen from Table 2 and Figure 4 that critical buckling loads can decrease considerably as the interfacial stiffness decreases.

However, this effect is insignificant if at least one among stiffnesses is high. Note that in the limiting case when at least one among stiffnesses tends to infinity, the critical buckling load becomes K and C independent. In this case, the critical buckling load of the CFST column corresponds to a total sum of the critical buckling loads of individual materials, namely the buckling load of the concrete core, $P^c_{\rm cr}$, and the steel tube, $P^s_{\rm cr}$, respectively,

$$P^*_{\rm cr} = P^c_{\rm cr} + P^s_{\rm cr} = \frac{\pi^2(E^cI^c + E^sI^s)}{(1+\varepsilon)L^2}, \tag{42}$$

and is therefore equivalent to P_E which is the Euler buckling load for the CFST column with perfectly bonded layers. On the contrary, in the limiting case when layers are fully debonded, it may be seen that the critical buckling load of the CFST column under consideration is

$$P^\bullet_{\rm cr} = P^c_{\rm cr} + P^s = \frac{\pi^2 E^c I^c}{(1+\varepsilon)L^2} + E^s A^s \varepsilon, \tag{43}$$

where P^s is the axial load carried by the steel tube. This result is expected since the critical buckling load of the concrete core in this particular case is almost as much as 3 times lower than the steel tube.

At the end of this example, first buckling modes of the individual layers c and s of the CFST P-P composite column are calculated for various K's and C's. The results are plotted in Figure 5.

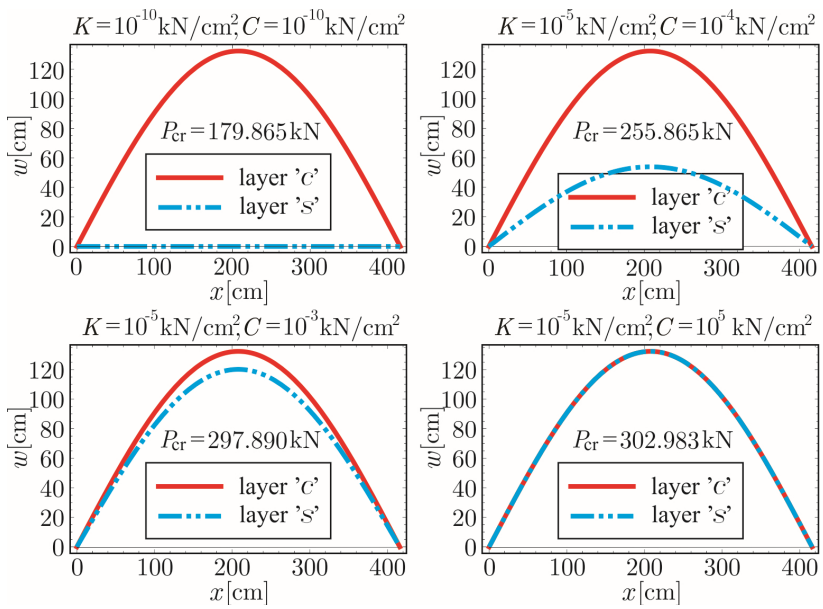

Figure 5: First buckling modes of layers c and s, and critical buckling loads of CFST P-P composite column for various values of K's and C's.

It can be seen from Figure 5 that in case of fully debonded materials, when K and C are almost negligible, only the concrete core buckles, while the steel tube remains straight. However, for all other values of K and C the deformations of the materials become constrained. This effect, however, becomes pronounced for rather rigidly connected materials in either of the two directions. Namely, in that case the first buckling modes of the two materials practically coincide.

3.3 Effect of Boundary Conditions on Buckling Loads

The effect of different boundary conditions on critical buckling loads of circular CFST composite columns is studied using the exact model developed. The effect is studied for the CFST column (i.e., specimen SC154-1) whose geometric and material properties are given in Figure 3 and Table 1.

The critical buckling loads of CFST columns are given in Table 3 for various K's and C's and different boundary conditions, i.e clamped-free (C-F), clamped-clamped (C-C), and clamped-pinned (C-P). Note, that the same boundary conditions are used for both materials, the concrete core and steel tube, respectively. As would be expected, the influence of interfacial compliance is similarly considerable in all cases of boundary conditions. The critical buckling loads decrease with the increase of interfacial compliance.

	P_{cr}					
C	10^{-10}			10^{-3}		
K	C-F	C-C	C-P	C-F	C-C	C-P
10^{-10}	44.95092961	719.2112490	367.8313917	75.13464138	1094.182170	590.2955496
10^{-5}	44.95989029	719.2202108	367.8403534	75.13465339	1094.183316	590.2958548
10^{-3}	45.83596664	720.1067487	368.7262276	75.13583959	1094.296689	590.3260369
10^{-2}	52.77689604	728.1035991	376.6569381	75.14637765	1095.317938	590.5973960
10^{-1}	71.11456051	801.7556923	443.5802350	75.23209327	1104.671332	593.0426878
1	75.25042232	1095.460050	588.7376543	75.50198900	1152.866275	604.9510316
10	75.65633017	1199.648599	616.4465577	75.66425898	1201.041703	616.7586267
10^{2}	75.69672750	1210.070051	619.1620639	75.69773741	1210.082508	619.1655195
10^{3}	75.70076519	1211.104568	619.4325425	75.70086471	1211.104691	619.4325774
10^{5}	75.70120931	1211.218272	619.4622827	75.70121211	1211.218272	619.4622827
10^{10}	75.70121379	1211.219421	619.4625831	75.70121379	1211.219421	619.4625831

Table 3: Critical buckling loads of circular CFST columns for various K, C, where $\lambda = 154$, $\varepsilon_{\text{cr}} = 0$, $E^c = 2760$ kN/cm^2, and C and K are in kN/cm^2.

4 CONCLUSIONS

The paper presented a new mathematical model for studying the buckling behaviour of circular CFST slender columns with compliant interfaces. The model is capable of predicting exact critical buckling loads and modes of CFST columns. The effect of interface compliance, and various other parameters, on critical buckling loads of CFST was studied in detail. Based on the results obtained in the present study, the following conclusions can be drawn:

1. The exact solution of the buckling loads of elastic circular CFST columns with compliant interface is presented.

2. A good agreement between the exact and experimental buckling loads of circular CFST composite columns is observed if at least one among longitudinal and radial interfacial stiffnesses is high. In the presence of finite interfacial compliance the critical buckling loads are reduced significantly.
3. The effect of interface compliance on critical buckling loads and modes of CFST columns is proved to be significant. The critical buckling loads decrease as the interfacial compliance increases. The first buckling modes proved to be constrained if a finite interfacial compliance is present.
4. As would be expected, the parametric study revealed that the critical buckling loads of circular CFST columns are also very much affected by the type of boundary conditions.
5. The results can be used as a benchmark solution for a buckling problem of circular CFST columns with compliant interfaces.

References

Aslani, F., Uy, B., Tao, Z., Mashiri, F., (2015). Behaviour and design of composite columns incorporating compact high-strength steel plates. Journal of Constructional Steel Research 107:94–110.

Brauns, J., (1999). Analysis of stress state in concrete-filled steel column. Journal of Constructional Steel Research 49:189–96.

Choi, K.K., Xiao, Y., (2010). Analytical studies of concrete-filled circular steel tubes under axial compression. Journal of Structural Engineering ASCE 136(5):565–73.

Dai, D.H., Lam, D., Jamaluddin, N., Ye, J., (2014). Numerical analysis of slender elliptical concrete filled columns under axial compression. Thin Walled Structures 77:26–35.

Ellobody, E., Young, B., Lam, D., (2006). Behaviour of normal and high strength concrete-filled compact steel tube circular stub columns. Journal of Constructional Steel Research 62(5):706–15.

Fam, A., Qie, F.S., Rizkalla, S., (2004). Concrete-filled steel tubes subjected to axial compression and lateral cyclic loads. Journal of Structural Engineering ASCE 130(4):631–40.

Feng, P., Cheng, S., Bai, Y., Ye, L., (2015). Mechanical behavior of concrete-filled square steel tube with FRP-confined concrete core subjected to axial compression. Computers and Structures 123:312–24.

Goode, C.D., Kuranovas, A., Kvedaras, A.K., (2010). Buckling of slender composite concrete-filled steel columns. Journal of Civil and Engineering Management 16(2):230–6.

Guo, L., Zhang, S., Kim, W.J., Ranzi, G., (2007). Behavior of square hollow steel tubes and steel tubes filled with concrete. Thin Walled Structures 45(12):961–973.

Hajjar, J.F., Schiller, P.H., Molodan, A., (1998). A distributed plasticity model for concrete-filled steel tube beam-columns with interlayer slip. Engineering Structures 20(8):663–76.

Han, L.H., (2000). Tests on concrete filled steel tabular columns with high slenderness ratio. Advances in Structural Engineering 3(4):337–44.

Han, L.H., Li, W., Bjorhovde, R., (2014). Developments and advanced applications of concrete-filled steel tubular (CFST) structures: Members. Journal of Constructional Steel Research 100:211–28.

Hassanein, M.F., Kharoob, O.F., (2014). Analysis of circular concrete-filled double skin tubular slender columns with external stainless steel tubes. Thin Walled Structures 79:23–37.

Hu, H.T., Huang, C.S., Wu, M.H., Wu, Y.M., (2003). Nonlinear analysis of axially loaded concrete-filled tube columns with confinement effect. Journal of Structural Engineering ASCE 129(10):1322–9.

Kryžanowski, A., Planinc, I., Schnabl, S., (2014). Slip-buckling analysis of longitudinally delaminated composite columns. Engineering Structures 76:404–14.

Kryžanowski, A., Schnabl, S., Turk, G., Planinc, I., (2008). Exact slip-buckling analysis of two-layer composite columns. International Journal of Solids and Structures 46:2929–38.

Kuranovas, A., Goode, D., Kvedaras, A.K., Zhong, S., (2009). Load-bearing capacity of concrete-filled steel columns. Journal of Civil Engineering and Management 15(1):21–33.

Lai M.H., Ho, J.C.M., (2014). Confinement effect of ring-confined concrete-filled-steel-tube columns under uni-axial load. Engineering Structures 67:123–41.

Liang, Q.Q., (2011). High strength circular concrete-filled steel tubular slender beam-columns, Part I: Numerical analysis. Journal of Constructional Steel Research 67:164–71.

Liao, F.Y., Han, L.H., He, S.h., (2011). Behavior of CFST short column and beam with initial concrete imperfection: Experiments. Journal of Constructional Steel Research 67(12):1922–35.

Patel, V.I., Liang, Q.Q., Hadi, M.N.S., (2014). Nonlinear analysis of axially loaded circular concrete-filled stainless steel tubular short columns. Journal of Constructional Steel Research 101:9–18.

Perko, L., (2001). Differential equations and dynamical systems, Springer-Verlag (New York).

Portolés, J.M., Romero, M.L., Filippou, F.C., Bonet, J.L., (2011). Simulation and design recommendations of eccentrically loaded slender concrete-filled tubular columns. Engineering Structures 33(5):1576–93.

Reissner, E. (1972). On one-dimensional finite-strain beam theory: The plane problem. Journal of Applied Mechanics and Physics, ZAMP 1972;23:795–804.

Roeder, C.W., Lehman, D.E., Bishop, E. (2010). Strength and stiffness of circular concrete-filled tubes. Journal of Structural Engineering ASCE 136(12):1545–53.

Romero, M.L., Moliner, V., Espinos, A., Ibañez, C., Hospitaler, A. (2011). Fire behavior of axially loaded slender high strength concrete-filled tubular columns. Journal of Constructional Steel Research 67(12):1953–65.

Schnabl, S., Planinc, I., (2010). The influence of boundary conditions and axial deformability on buckling behavior of two-layer composite columns with interlayer slip. Engineering Structures 32(10):3103–11.

Schnabl, S., Planinc, I., (2011a). The effect of transverse shear deformation on the buckling of two-layer composite columns with interlayer slip. International Journal of Nonlinear Mechanics 46(3):543–53.

Schnabl, S., Planinc, I., (2011b). Inelastic buckling of two-layer composite columns with non-linear interface compliance. International Journal of Mechanical Sciences 53(12):1077–83.

Schnabl, S., Planinc, I., (2013). Exact buckling loads of two-layer composite Reissner's columns with interlayer slip and uplift. International Journal of Solids and Structures 50:30–7.

Schnabl, S., Planinc, I., (2015). Analytical buckling of slender circular concrete-filled steel tubular columns with compliant interfaces. Journal of Constructional Steel Research 115:252–62.

Schnabl, S., Saje, M., Turk, G., Planinc, I., (2007). Analytical solution of two-layer beam taking into account interlayer slip and shear deformation. Journal of Structural Engineering ASCE 133(6):866–94.

Schneider, S., (1998). Axially loaded concrete-filled steel tubes. Journal of Structural Engineering ASCE 124(10):1125–38.

Shams, M., Saadeghvaziri, M.A., (1999). Nonlinear response of concrete-filled steel tubular columns under axial loading. Journal of Constructional Steel Research 96(6):1009–17.

Shanmugam, N.E., Lakshmi, B., (2001). State of the art report on steel-concrete composite columns. Journal of Constructional Steel Research 57:1041–80.

Susantha, K.A.S., Ge, H., Usami, T. (2001). Uniaxial stress-strain relationship of concrete confined by various shaped steel tubes. Engineering Structures 23:1331–47.

Tao, Z., Wang, Z.B., Yu, Q., (2013). Finite element modelling of concrete-filled steel stub columns under axial compression. Journal of Constructional Steel Research 89:121–31.

Valipour, H.R., Foster, S.J., (2010). Nonlinear analysis and cyclic analysis of concrete-filled steel columns. Journal of Constructional Steel Research 66:793–802.

Wang, K., Young, B., (2013). Fire resistance of concrete-filled high strength steel tubular columns. Thin Walled Structures 71:46–56.

Wang, Y., Chen, J., Geng, Y., (2015). Testing and analysis of axially loaded normal-strength recycled aggregate concrete filled steel tubular stub columns. Engineering Structures 86:192–212.

Yang, Y.F., Han, L.H., (2006). Experimental behaviour of recycled aggregate concrete filled steel tubular columns. Journal of Constructional Steel Research 62:1310–24.

Zeghiche, J., Chaoui, K., (2005). An experimental behaviour of concrete-filled steel tubular columns. Journal of Constructional Steel Research 61:53–66.

Zhang, D.J., Ma, Y.S., Wang, Y., (2015). Compressive behavior of concrete filled steel tubular columns subjected to long-term loading. Thin Walled Structures 89:205–11.